Schizophrenia Research 169 (2015) 36–45

Contents lists available at ScienceDirect

Schizophrenia Research

journal homepage: www.elsevier.com/locate/schres

Subcomponents of brain T2* relaxation in schizophrenia, bipolar disorder and siblings: A Gradient Echo Plural Contrast Imaging (GEPCI) study

Daniel Mamah [a,*], Jie Wen [b], Jie Luo [b], Xialing Ulrich [b], Deanna M. Barch [a,c,d], Dmitriy Yablonskiy [b]

[a] Department of Psychiatry, Washington University Medical School, St. Louis, United States
[b] Department of Radiology, Washington University Medical School, St. Louis, United States
[c] Department of Psychology, Washington University in St. Louis, United States
[d] Department of Anatomy and Neurobiology, Washington University in St. Louis, United States

ARTICLE INFO

Article history:
Received 3 August 2015
Received in revised form 2 October 2015
Accepted 6 October 2015
Available online 23 October 2015

Keywords:
Schizophrenia
Bipolar
Siblings
GEPCI
T2*
MRI
Brain
Relaxometry

ABSTRACT

Investigating brain tissue T2* relaxation properties in vivo can potentially guide the uncovering of neuropathology in psychiatric illness, which is traditionally examined post mortem. We use an MRI-based Gradient Echo Plural Contrast Imaging (GEPCI) technique that produces inherently co-registered images allowing quantitative assessment of tissue cellular and hemodynamic properties. Usually described as R2* (=1/T2*) relaxation rate constant, recent developments in GEPCI allow the separation of cellular-specific ($R2^*_C$) and hemodynamic (BOLD) contributions to the MRI signal decay. We characterize BOLD effect in terms of tissue concentration of deoxyhemoglobin, i.e. C_{DEOXY}, which reflects brain activity. 17 control (CON), 17 bipolar disorder (BPD), 16 schizophrenia (SCZ), and 12 unaffected schizophrenia sibling (SIB) participants were scanned and post-processed using GEPCI protocols. A MANOVA of 38 gray matter regions ROIs showed significant group effects for C_{DEOXY} but not for $R2^*_C$. In the three non-control groups, 71–92% of brain regions had increased C_{DEOXY}. Group effects were observed in the superior temporal cortex and the thalamus. Increased superior temporal cortex C_{DEOXY} was found in SCZ ($p = 0.01$), BPD ($p = 0.01$) and SIB ($p = 0.02$), with bilateral effects in SCZ and only left hemisphere effects in BPD and SIB. Thalamic C_{DEOXY} abnormalities were observed in SCZ ($p = 0.003$), BPD ($p = 0.03$) and SIB ($p = 0.02$). Our results suggest that increased activity in certain brain regions is part of the underlying pathophysiology of specific psychiatric disorders. High C_{DEOXY} in the superior temporal cortex suggests abnormal activity with auditory, language and/or social cognitive processing. Larger studies are needed to clarify the clinical significance of relaxometric abnormalities.

1. Introduction

To date, existing neuroimaging methods including structural, functional and diffusion magnetic resonance imaging (MRI) have not had significant clinical applications in psychiatry. While these methods are highly informative, they provide a limited understanding of tissue abnormalities more proximal to the respective modality based findings. Characterizing such intrinsic abnormalities could provide clues to understanding etiologic mechanism in psychiatric disorders, such as schizophrenia and bipolar disorder. The reported post mortem neuropathology of these disorders have been somewhat inconsistent across studies (Arnold and Trojanowski, 1996; Selemon, 2001). Studies in schizophrenia for example, find a general lack of neurodegenerative disease lesions or ongoing astrocytosis that would indicate post-maturational neural injury (Arnold et al., 1996; Casanova et al., 1990; Roberts et al., 1986; Stevens et al., 1988), however neuronal apoptosis has been reported (Glantz et al., 2006; Jarskog et al., 2005). Decreased size of neuronal cell bodies (Cotter et al., 2005; Elston and Rosa, 1998; Hayes and Lewis, 1996; Ho et al., 1992; Pierce and Lewin, 1994) and/or neural processes and dendritic spines (Garey, 2010) are sometimes present in schizophrenia and bipolar disorder, as well as increased neuronal density (Schlaug et al., 1993) as neurons pack more closely together. Other authors found no changes in neuronal density (Arnold, 2000; Cullen et al., 2006) or reduced neuronal (Di Rosa et al., 2009; Rajkowska et al., 2001) or glial cell (Cotter et al., 2001; Rajkowska et al., 2001) density.

In this paper, we use an advanced version (Ulrich and Yablonskiy, 2015) of Gradient Echo Plural Contrast Imaging (GEPCI) technique (Luo et al., 2012; Yablonskiy, 2000) to study brain tissue cellular and hemodynamic neuropathology in psychiatric disorders, which is traditionally examined post mortem. The GEPCI technique is mainly based on quantitative measurements of the transverse relaxation (R2*, i.e. 1/T2*) properties of the gradient echo MRI signal. Since gradient echo images are affected by artifacts related to background gradients and physiological fluctuations, we use two correction methods to minimize these adverse effects — voxel spread function

* Corresponding author at: Department of Psychiatry, Washington University Medical School, 660 S. Euclid, Saint Louis, MO 63110, United States.
E-mail address: mamahd@psychiatry.wustl.edu (D. Mamah).

http://dx.doi.org/10.1016/j.schres.2015.10.004
0920-9964/

(VSF) approach (Yablonskiy et al., 2013b) and f_0 correction method (Wen et al., 2014). Recent developments using GEPCI have allowed the separation of tissue components that make up the R2* signal decay into cellular ($R2^*_C$) and blood-oxygen-level dependent (BOLD) contributions (Ulrich and Yablonskiy, 2015), thus promising more elaborate descriptions of tissue properties in disease. $R2^*_C$ describes part of the R2* decay resulting from water molecules' interaction with cellular components of biological tissues, and can thus serve as a biomarker indicating "cellular health", and is sensitive to cellular alterations in the brain. The BOLD contribution comes from the presence of deoxyhemoglobin in the blood (Ogawa, 2012). Herein we use the previously developed theory of the BOLD effect (Yablonskiy and Haacke, 1994) that predicted non-linear dependence of MRI signal transverse relaxation on gradient echo time, thus allowing separation of cellular and BOLD contributions (Yablonskiy, 1998). Separating the non-linear MRI signal decay due to the BOLD effect could provide important information on tissue metabolic properties which are important for understanding normal human brain operation (Raichle and Mintun, 2006) as well as the pathophysiology of brain disease (Derdeyn et al., 2002; Iadecola, 2004). Specifically, in this paper we will characterize the resting state BOLD effect in terms of the tissue concentration of deoxyhemoglobin C_{DEOXY}. An increase in tissue C_{DEOXY} in a brain region would indicate insufficient oxygen supply compared to demand, which relates to increased activity and/or metabolism. In contrast, decreased C_{DEOXY} implies decreased oxygen utilization.

In previous studies, GEPCI has been used to investigate patients with multiple sclerosis (MS) (Luo et al., 2012; Luo et al., 2014; Sati et al., 2010; Wen et al., 2014; Wen et al., 2015; Yablonskiy et al., 2012), with findings of decreased R2* relaxation in white matter, consistent with the characteristic myelin and/or axonal loss and inflammation. Results also showed that GEPCI-derived R2* metrics correlated better with neurologic disability and tissue damage than lesion load derived using a conventional MRI acquisition (Luo et al., 2014; Sati et al., 2010; Wen et al., 2014; Wen et al., 2015). Studies using the quantitative methods of GEPCI have not been previously conducted for psychiatric disorders. In the current exploratory study, we apply GEPCI techniques to participants with schizophrenia and bipolar disorder, two of the potentially most disabling psychiatric illnesses (Whiteford et al., 2013). Our study population also includes unaffected siblings of those with schizophrenia, in order to investigate genetic markers of disease without the influence of medications. We analyze tissue characteristics of white and gray matter using subcomponents contributing to the R2* signal decay, specifically, $R2^*_C$ (characterizing tissue cellular properties) and C_{DEOXY} (characterizing tissue hemodynamic properties), to uncover specific illness pathomechanisms. Results of our study shed light on the application of this new methodology in psychiatry, and show a potential to guide the field towards a better understanding of psychiatric neurobiology.

2. Materials and methods

2.1. Participants

Participant groups included: 1) healthy controls (CON; N = 17); 2) bipolar disorder (BPD; N = 17); 3) schizophrenia (SCZ; N = 16); and 4) siblings of individuals with SCZ who did not have a diagnosis of SCZ or BPD or any other DSM-IV psychotic disorder (SIB; N = 12). Participants' ages ranged between 19 and 50 yrs. Table 1 shows demographic and clinical data across the four participant groups. All participants gave written informed consent for participation. SCZ and BPD participants were all outpatients, and clinically stable for at least two weeks. They were diagnosed on the basis of a consensus between a research psychiatrist and a trained research assistant who used the Structured Clinical Interview for DSM-IV Axis I Disorder. CON subjects were required to have no lifetime history of DSM-IV Axis I psychotic or mood disorders. SCZ, BPD and SIB participants did not have psychotic or mood disorder histories other than their primary diagnosis. DSM-IV Axis II disorders were not investigated. Participants were excluded if they: (a) met DSM-IV criteria for substance dependence or severe/moderate abuse during the prior 6 months; (b) had a clinically unstable or severe general medical disorder; or (c) had a history of head injury with documented neurological sequelae or loss of consciousness. The study was approved by Washington University's Institutional Review Board.

Table 1
Demographics and clinical data table.

Characteristics	CON (n = 17)	BPD (n = 17)	SCZ (n = 16)	SIB (n = 12)
Mean age (SD)	35.6 (8.1)	26.1 (3.2)	35.8 (8.5)	31.3 (8.6)
Gender (%)				
Female	58.8	82.4	31.3	66.7
Male	41.2	17.6	68.7	33.3
Race (%)				
Black	64.7	5.9	50.0	33.3
White	35.3	94.1	50.0	66.7
History of use disorder (%)[a]				
Nicotine	29.4	41.2	68.8	33.3
Alcohol	5.9	35.3	31.3	16.7
Cannabis	5.9	23.5	31.3	8.3
Stimulant	–	5.9	6.3	–
Opioid	–	–	6.3	–
Cocaine	5.9	–	6.3	–
Hallucinogen	–	–	6.3	–
Psychotropic medication (%)				
Typical neuroleptic	–	–	12.5	–
Atypical neuroleptic	–	41.2	81.3	–
SSRI	–	29.4	18.8	–
Other antidepressants [b]	–	23.5	18.8	–
Mood stabilizer	–	47.1	31.3	–
Benzodiazepines	–	11.8	12.5	–
Stimulant	–	17.6	–	–
Anticholinergic	–	–	18.8	–
None	100.0	29.4	12.5	100.0
Symptom domains[c]				
SAPS	0.29 (0.8)	2.59 (2.6)	4.94 (3.5)	0.50 (0.9)
Positive symptoms[d]	0.06 (0.2)	1.00 (1.4)	3.75 (2.4)	0.08 (0.3)
Disorganized symptoms[d]	0.24 (0.7)	1.59 (1.6)	1.19 (1.7)	0.42 (0.8)
SANS[e]	2.29 (2.8)	2.59 (3.5)	7.94 (3.2)	2.92 (2.7)

[a] Other than for nicotine use disorder, participants did not meet criteria for a use disorder in the last 6 months.
[b] Refers to antidepressants other than selective serotonin reuptake inhibitors (SSRI).
[c] Values given as means (SD).
[d] Positive and Disorganized Symptoms were derived from the Structured Assessment of Positive Symptoms (SAPS). Maximum possible score on the SAPS is 16; and either positive or disorganized symptoms is 8.
[e] Maximum possible score on the Structured Assessment of Negative Symptoms (SANS) is 20.

2.2. Clinical assessment

Psychopathology was assessed using the Scale for the Assessment of Negative Symptoms (SANS) and the Scale for the Assessment of Positive Symptoms (SAPS) (Andreasen et al., 1995). Specific subscale scores were summed to derive measures of positive symptoms (i.e. hallucination and delusion subscales), disorganization (i.e. formal thought disorder, bizarre behavior and attention subscales), and negative symptoms (i.e. flat affect, alogia, anhedonia and amotivation subscales). Table 1 shows mean SAPS and SANS scores across groups.

2.3. MRI scanning

All scanning occurred on a 3 T Tim TRIO Scanner at Washington University Medical School.

GEPCI data were obtained using a 3D version of the multi-gradient echo sequence with a resolution = 1 × 1 × 3 mm^3, FOV = 256 × 192 × 120 mm^3, and 11 gradient echoes (min TE = 4 ms; delta-TE = 4 ms; TR = 50 ms; bandwidth = 510 Hz/Pixel; FA = 30°) was used, with a total acquisition time of 6.4 min. Additional phase stabilization echo (the navigator data) was collected for each line in k-space to correct for image artifacts due to the physiological fluctuations (Wen et al., 2014). Effects of field inhomogeneities (background gradients) were removed using the voxel spread function (VSF) approach (Yablonskiy et al., 2013b).

2.4. Generating GEPCI images

Image processing was finished in MATLAB (The MathWorks, Inc.) using previously developed algorithms. In brief, images were generated after correcting the k-space data for physiological artifacts (Wen et al., 2014). 3D spatial Hanning filter was then applied to the data in the image domain. To achieve an optimal signal-to-noise ratio, we use the following equation to combine the data of all channels (Luo et al., 2012):

$$S_n(\mathrm{TE}) = \sum_{ch=1}^{M} \lambda_{ch} \cdot \overline{S}_n^{ch}(\mathrm{TE}_1) \cdot S_n^{ch}(\mathrm{TE}); \quad \lambda_{ch} \frac{1}{M \cdot \varepsilon_{ch}^2} \sum_{ch=1}^{M} \varepsilon_{ch}^2 \tag{1}$$

where the sum is taken over all M channels (ch). $\overline{S}$ denotes complex conjugate of S, λ_{ch} are weighting parameters, ε_{ch} are noise amplitudes (r.m.s.), and the index n corresponds to the voxel position (n = x,y,z). This algorithm allows for the optimal estimation of quantitative parameters, and also removes the initial phase incoherence among the channels (Luo et al., 2012; Quirk et al., 2009).

The data were then analyzed on a voxel-by-voxel basis using theoretical model (Yablonskiy, 1998):

$$S(\mathrm{TE}) = A_0 \cdot \exp(-\mathrm{R2}*_C \cdot \mathrm{TE} + i \cdot 2\pi \cdot \Delta f \cdot \mathrm{TE}) \cdot F_{\mathrm{BOLD}}(\mathrm{TE}) \cdot F(\mathrm{TE}) \tag{2}$$

where TE is the gradient echo time, $R2^*_C = 1/T2^*_C$ is the tissue cellular transverse relaxation rate constant (describing GRE signal decay in the absence of BOLD effect), Δf is the frequency shift (dependent on tissue structure and also macroscopic magnetic field created mostly by tissue/air interfaces), function $F_{\mathrm{BOLD}}(\mathrm{TE})$ describes GRE signal decay due to the presence of blood vessel network with deoxygenated blood (veins and adjacent to them part of capillaries), and function $F(\mathrm{TE})$ describes the effects of macroscopic magnetic field inhomogeneities. We used the voxel spread function (VSF) method (Yablonskiy et al., 2013b) for calculating $F(\mathrm{TE})$. For the BOLD model we used the following expression (Ulrich and Yablonskiy, 2015):

$$F_{\mathrm{BOLD}}(\mathrm{TE}) = 1 - \frac{\zeta}{1-\zeta} \cdot f_s(\delta\omega \cdot \mathrm{TE}) + \frac{1}{1-\zeta} \cdot f_s(\zeta \cdot \delta\omega \cdot \mathrm{TE}) \tag{3}$$

where the function f_s describes the signal decay due to the presence of blood vessel network and was defined in Yablonskiy and Haacke (1994).

Eq. (3) better accounts for the presence of large vessels in the voxel than traditional exponential function (Yablonskiy and Haacke, 1994). Here, ζ is the deoxygenated cerebral blood volume fraction (dCBV) and $\delta\omega$ is the characteristic frequency determined by the susceptibility difference between deoxygenated blood and surrounding tissue (Yablonskiy and Haacke, 1994):

$$\delta\omega = \frac{4}{3}\pi \cdot \gamma \cdot B_0 \cdot \mathrm{Hct} \cdot \Delta\chi_0 \cdot (1-Y) \tag{4}$$

In this equation, $\Delta\chi_0 = 0.27$ ppm (Spees et al., 2001) is the susceptibility difference between fully oxygenated and fully deoxygenated blood, Y is the blood oxygenation level (with $Y = 0$ being fully deoxygenated, and $Y = 1$ being fully oxygenated), Hct is the blood hematocrit, and γ is the gyromagnetic ratio. Herein we use a mathematical expression for the function f_s in terms of a generalized hypergeometric function ${}_1F_2$ (Yablonskiy et al., 2013a):

$$f_s(\delta\omega \cdot \mathrm{TE}) = {}_1F_2\left(\left[-\frac{1}{2}\right]; \left[\frac{3}{4}, \frac{5}{4}\right]; -\frac{9}{16}(\delta\omega \cdot \mathrm{TE})^2\right) - 1 \tag{5}$$

By fitting Eq. (2) to the complex signal using nonlinear regression algorithm, we are able to generate the five parameters: S_0, $R2^*_C$, Δf, ζ and $\delta\omega$ for each voxel in the brain. Details of the fitting routine have been described in great detail (Ulrich and Yablonskiy, 2015).

Based on the above-described parameters we can also calculate the concentration of deoxyhemoglobin per unit tissue volume (He and Yablonskiy, 2007):

$$C_{\mathrm{deoxy}} = \zeta \cdot n_{Hb} \cdot \mathrm{Hct} \cdot (1-Y) = \frac{3}{4} \cdot \frac{\zeta \cdot \delta\omega \cdot n_{Hb}}{\gamma \cdot \pi \cdot \Delta\chi_0 \cdot B_0} \tag{6}$$

where n_{Hb} is the total intracellular concentration of hemoglobin equal to 5.5×10^{-6} mol/mL (He and Yablonskiy, 2007).

2.5. Image segmentation

FreeSurfer (Martinos Center for Biomedical Imaging, Charlestown, MA) was used to generate brain segmentations from MPRAGE images, deriving 38 cortical and subcortical regions of interest (ROIs). MPRAGE images were registered to GEPCI-T1-weighted images using FMRIB's Linear Image Registration Tool (Jenkinson et al., 2002; Jenkinson et al., 2012) in FSL (University of Oxford, UK) and the transformation matrices of the registration were generated. These matrices were applied to the brain segmentations from FreeSurfer and transformed to the space of GEPCI-T1-weighted images. Since GEPCI-T1-weighted images are naturally co-registered to all other GEPCI-generated parameters (i.e. $R2^*_C$ and C_{DEOXY}), the segmentations were also naturally registered.

2.6. Post-processing and statistical analyses

Statistical analyses were established using MATLAB (The MathWorks, Inc.) and SAS 9.4 (SAS Institute Inc., Cary, NC). $R2^*_C$ and C_{DEOXY} values for each ROI were defined as the median voxel values within that ROI. $R2^*_C$ and C_{DEOXY} were normally distributed (Shapiro–Wilk: $p = 0.15$–0.78) in each ROI, with the exception of thalamus C_{DEOXY} in SCZ and SIB. A Levene's test assessing the homogeneity of variance across diagnostic groups was insignificant for most comparisons, with the exception of thalamic C_{DEOXY} between CON and SCZ. White matter $R2^*_C$ differences between subjects of different diagnostic groups were tested using Analysis of Variance (ANOVA) with and without covarying for age. Multivariate Analysis of Covariance (MANCOVA) was used to test group differences in gray matter involving multiple brain regions-of-interest (ROIs). Alpha was set at 0.05. Post-hoc comparisons of individual gray matter regions were done using ANOVA, with and without covarying for age. For thalamic C_{DEOXY} comparisons a logarithmic ($\log_{10}$) transformation was applied to correct for non-normality and unequal variances. Hemispheric effects were investigated for ROIs using repeated measures ANOVA, controlled for age, with hemisphere as the repeated measure. As thalamic C_{DEOXY} values in some groups were not normally distributed, for uniformity Spearman's correlation was used to test C_{DEOXY} relationships with clinical domains derived from the SAPS and SANS assessments, partialing out diagnosis and age. Clinical relationships were investigated across all groups, and in patient groups only (i.e. in SCZ and BPD).

3. Results

3.1. White matter relaxation

Least square means (age-corrected) of the total white matter median $R2^*_C$ values were (in s^{-1}): 19.2 in CON, 19.2 in BPD, 19.1 in SCZ, and 19.6 in SIB. The effect of diagnosis was not statistically significant ($p = 0.3$).

3.2. Regional gray matter relaxation

$R2^*_C$ and C_{DEOXY} group z-score means (SD) of the 38 gray matter ROIs parcellated using FreeSurfer are graphically depicted in Fig. 1, and represented on the cortical surface in Fig. 2.

3.2.1. $R2^*_C$ relaxation

Result using a MANOVA of the 38 age-corrected median $R2^*_C$ values was non-significant (Wilk's $\lambda = 0.03$; $p = 0.3$). Figs. 1A and 2A depict group means of $R2^*_C$ across ROIs. Of note, in SCZ almost all ROIs had lower $R2^*_C$ than CON.

3.2.2. C_{DEOXY}

C_{DEOXY} median values used as dependent variables in an age-corrected MANCOVA showed significant omnibus group effects (Wilk's $\lambda = 0.02$; $p = 0.035$). Table 2 shows C_{DEOXY} values across groups and ANOVA results. As seen in Figs. 1B and 2B, mean C_{DEOXY} showed a tendency towards increased values in all three non-control groups. The percentage of ROIs with increased mean C_{DEOXY} compared to CON was 92.1% for SCZ, 71.1% for BPD and 81.6% for SIB.

In post-hoc analyses, C_{DEOXY} group differences were only significant in the superior temporal cortex ($F = 3.5$; $p = 0.021$) and the thalamus ($F = 2.8$; $p = 0.049$). For individual superior temporal cortex comparisons, correcting for age, significant effects were found between CON v. SCZ ($p = 0.01$), CON v. BPD ($p = 0.01$) and CON v. SIB ($p = 0.02$) with increased mean C_{DEOXY} in the three non-control groups (Fig. 1B, Table 2). Results of analyses were similar when corrected for age; however CON v. BPD results were significant only at trend level ($p = 0.06$). Following a logarithmic transformation of thalamus C_{DEOXY} values to adjust for differences in variance heterogeneity, comparisons (corrected for age) were highly significant between CON v. SCZ ($p = 0.003$), CON v. BPD ($p = 0.03$), and CON v. SIB ($p = 0.02$) with increased mean thalamic C_{DEOXY} in SCZ, BPD and SIB. All thalamic comparisons were similarly significant when analyses were not corrected for age.

3.2.3. Hemispheric effects

We explored hemispheric C_{DEOXY} differences in the superior temporal cortex and the thalamus, which showed significant group effects (Fig. 3).

There was a significant hemispheric effect ($p = 0.03$) for superior temporal cortex C_{DEOXY} but no group × hemisphere effect. Right superior

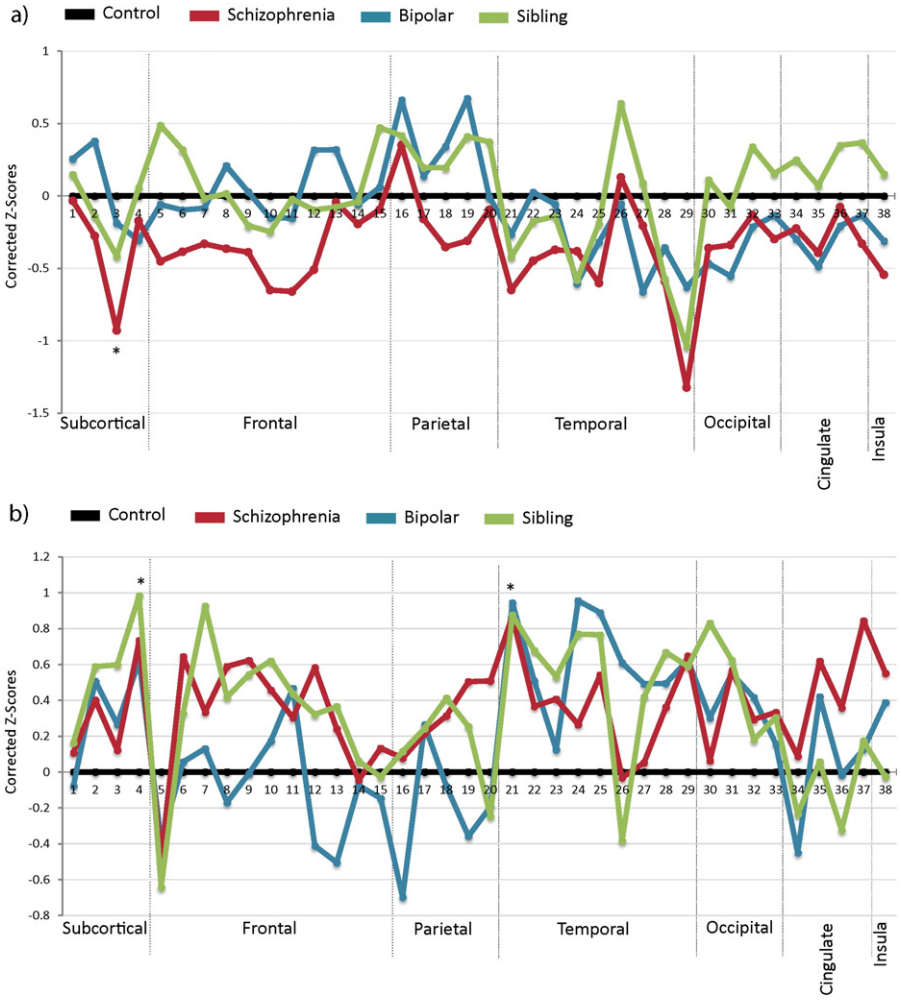

Fig. 1. Line graphs of regional $R2^*_C$ and C_{DEOXY} by group. Graphs depict corrected z-scores of $R2^*_C$ (A), and C_{DEOXY} (B) values averaged for the four participant groups: healthy controls, bipolar disorder, schizophrenia, and the unaffected siblings of schizophrenia patients. z-Scores were corrected for age, and group means normalized against the control group. Values are derived from the each participants median $R2^*_C$ or C_{DEOXY} voxel values. ROI numbers correspond to regions listed in Table 2. Asterisks represent ROIs where post-hoc ANOVA resulted in statistical significance of $p < 0.05$.

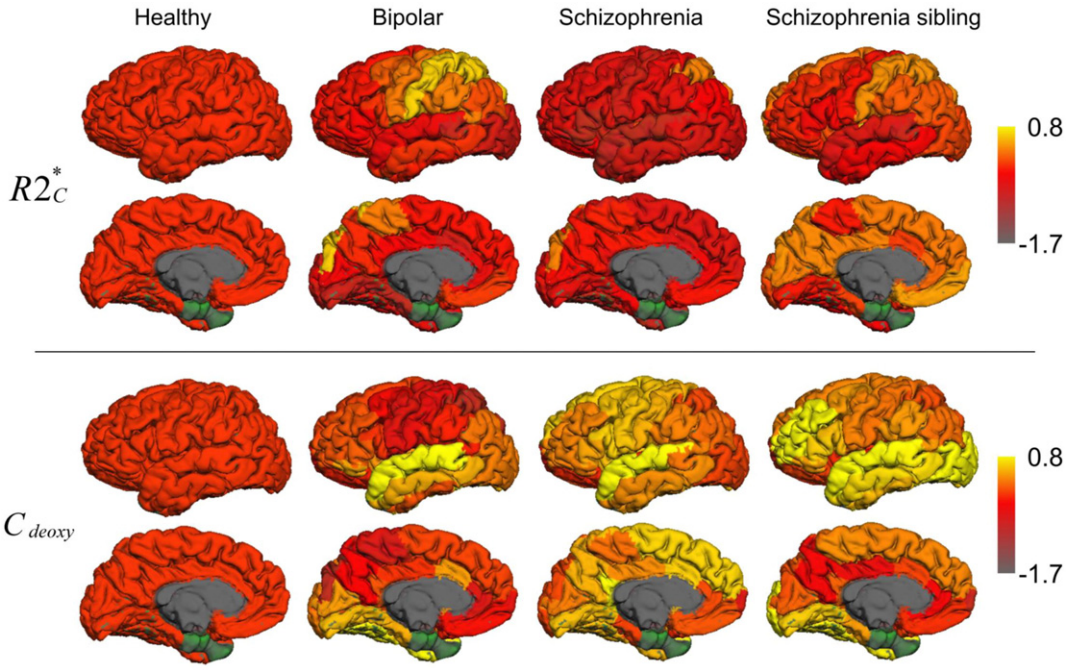

Fig. 2. Cortical surface depiction of $R2^*_C$ and C_{DEOXY} by group. Surface maps depict mean $R2^*_C$ (top), and C_{DEOXY} (bottom) corrected z-scores projected onto cortical ROIs. z-Scores were corrected for age, and group means normalized against the control group. Subcortical ROIs are not depicted. ROIs in green (i.e. entorhinal cortex and temporal pole) were not included in our analyses, as complete GEPCI coverage of these regions was not obtained in a substantial number of participants.

temporal cortex C_{DEOXY} was slightly higher than the left in CON and SCZ, with the opposite finding in BPD. On the left, superior temporal cortex significant group differences were found between CON v. SCZ ($p = 0.048$), CON v. BPD ($p = 0.04$), and CON v. SIB ($p = 0.04$). On the right, superior temporal cortex significant group effects were only found between CON v. SCZ ($p = 0.02$), while there was a trend level effect between CON v. SIB ($p = 0.1$).

There were no significant hemispheric effects for the thalamus. Thalamus C_{DEOXY} values were significantly different for both hemispheres between CON v. SCZ (left: $p = 0.03$; right: $p = 0.01$), CON v. BPD (left: $p = 0.05$; right: $p = 0.04$), and CON v. SIB (left: $p = 0.003$; right: $p = 0.03$).

3.3. Correlations between clinical and radiological measurements

We studied the relationships of clinical symptoms derived from the Structured Assessment of Positive Symptoms (SAPS) and the Structured Assessment of Negative Symptoms (SANS) with C_{DEOXY} values in the superior temporal cortex and the thalamus. When studied across groups, a significant direct correlation was observed between C_{DEOXY} in the thalamus and positive symptom domain scores on the SAPS ($r = 0.26$; $p = 0.04$). Additionally, a trend level of significance was noted for correlations between C_{DEOXY} in the superior temporal cortex and disorganization symptom domain scores on the SAPS ($r = 0.22$; $p = 0.097$). When only SCZ or both SCZ and BPD were investigated, there were no significant correlations observed for either region with any of the clinical domains.

4. Discussion

Results from our studies demonstrate, for the first time, the utility of the Gradient Echo Plural Contrast Imaging (GEPCI) (Luo et al., 2012; Yablonskiy, 2000) in the quantitative study of brain relaxation properties in psychiatric populations. By applying two recently developed correction methods (Wen et al., 2014; Yablonskiy et al., 2013b) that minimize artifacts related to macroscopic magnetic field inhomogeneities and physiological fluctuations, GEPCI allows obtaining tissue-specific measurements characterizing cellular and hemodynamic tissue properties. Being quantitative, GEPCI provides measures that are not influenced by differences in pulse sequences, and thus are less intersite dependent than those acquired using standard weighted imaging (Ropele et al., 2013; Weiskopf et al., 2013). Our findings suggest that uncoupling subcomponents of R2* relaxation into cellular ($R2^*_C$) and extravascular BOLD contributions (Ulrich and Yablonskiy, 2015) to the GRE signal decay can provide useful information for understanding pathomechanisms of psychiatric illnesses.

Significant relaxometric findings in our study pertained to C_{DEOXY}, which showed group differences in several brain gray matter regions. C_{DEOXY} represents the deoxyhemoglobin status in veins (Ulrich and Yablonskiy, 2015) and thus is expected to reflect a balance between oxygen supply and consumption required for brain activity and/or metabolism, with increased C_{DEOXY} indicating imbalance towards increased oxygen consumption with insufficient oxygen supply. While C_{DEOXY} values varied across brain regions, we observed a tendency for findings, particularly in schizophrenia (SCZ), to be higher than that in the control group. C_{DEOXY} group differences in a smaller majority of gray matter regions were also higher in bipolar disorder (BPD) and unaffected schizophrenia siblings (SIB). Most of these findings however, did not meet statistical significance, but were notable as they represented a pattern that was evident in all three non-control populations. Importantly, it may imply a generalized, although largely modest, brain hypermetabolism associated with certain psychopathological states. Significant C_{DEOXY} group differences from controls were found in the superior temporal cortex and the thalamus, with increases in SCZ, BPD and SIB. While thalamic abnormalities were present bilaterally in each non-control group, superior temporal cortex abnormalities were bilateral only in SCZ, with BPD and SIB participants showing only left hemisphere effects. The relevance of these disparate hemispheric effects is unclear. The left superior temporal gyrus in most people unilaterally consists of Wernicke's area that is involved in

Table 2
C_{DEOXY} median values by region.

Predominant Brain zone	ROI	CON	BPD	SCZ	SIB	p
Subcortical	1. Caudate	45.44	44.63	46.57	47.15	0.92
	2. Putamen	37.24	41.88	40.91	42.61	0.40
	3. Globus pallidus	50.16	53.42	51.66	57.49	0.47
	4. Thalamus*	22.76	26.19	26.82	28.21	0.05*
Frontal	5. Frontal pole	100.88	92.54	90.38	87.03	0.35
	6. Superior frontal	26.55	26.83	29.76	28.19	0.27
	7. Rostral middle frontal	30.38	31.29	32.72	36.88	0.08
	8. Caudal middle frontal	24.35	23.53	27.19	26.37	0.14
	9. Pars opercularis	31.17	31.12	35.40	34.87	0.16
	10. Pars triangularis	39.01	40.83	43.83	45.53	0.34
	11. Pars orbitalis	53.16	60.28	57.79	59.78	0.61
	12. Precentral	25.92	24.04	28.57	27.38	0.05
	13. Paracentral	23.38	20.84	24.60	25.22	0.11
	14. Lateral orbitofrontal	70.82	69.84	70.23	71.61	0.99
	15. Medial orbitofrontal	91.99	89.66	94.11	91.56	0.92
Parietal	16. Superior parietal	24.65	21.82	24.96	25.11	0.11
	17. Inferior parietal	21.78	22.56	22.41	22.50	0.89
	18. Supramarginal	26.09	25.75	27.42	27.84	0.50
	19. Postcentral	27.88	26.26	30.17	29.03	0.13
	20. Precuneus	20.17	19.71	21.36	19.59	0.19
Temporal	21. Superior temporal*	47.16	54.38	53.81	53.86	0.02*
	22. Middle temporal	48.53	53.80	52.34	55.56	0.34
	23. Inferior temporal	44.12	45.76	49.47	51.12	0.46
	24. Banks sup. temp. sulcus	23.53	30.33	25.42	29.00	0.06
	25. Fusiform	26.79	32.08	30.00	31.35	0.09
	26. Transverse temporal	48.41	53.91	48.13	44.96	0.07
	27. Parahippocampal	40.21	45.10	40.73	44.37	0.52
	28. Hippocampus	39.44	44.16	42.89	45.82	0.35
	29. Amygdala	56.94	67.01	67.34	66.45	0.21
Occipital	30. Lateral occipital	29.05	30.56	29.37	33.18	0.15
	31. Lingual	23.84	26.30	26.38	26.64	0.28
	32. Cuneus	21.03	22.41	22.00	21.63	0.72
	33. Pericalcarine	20.93	21.60	22.34	22.23	0.79
Cingulate	34. Rostral ant. cingulate	68.39	60.93	69.86	64.50	0.55
	35. Caudal ant. cingulate	29.92	32.36	33.50	30.24	0.25
	36. Posterior cingulate	24.59	24.51	26.31	23.04	0.39
	37. Isthmus of cingulate	20.54	20.97	23.40	21.13	0.08
Insula	38. Insula	38.55	40.82	41.82	38.40	0.29

Values listed represented least squared means of the median C_{DEOXY} in each region, after correction for age. C_{DEOXY} values are given in μM. Asterisks indicate regions showing significant ($p < 0.05$) group differences using an ANCOVA corrected for age.

language comprehension (Karnath, 2001), and may be more susceptible to impairment than the right. Our findings indicate that abnormalities in SCZ are more severe, as they involve both hemispheres. The regions found to be abnormal in our study are consistent with existing knowledge about brain abnormalities in SCZ. One of the most commonly implicated regions in imaging studies of SCZ is the superior temporal gyrus (STG) (Honea et al., 2005; Pearlson, 1997; Sun et al., 2009), and it is also involved in key functions that are thought to be impaired in the disorder. The STG contains the transverse temporal gyrus (i.e. Heschl's gyrus) in the area of the primary auditory cortex, which is responsible for processing of sound. The STG also contains several important network of connections to temporal limbic brain regions which plays a major role in the production, interpretation and self-monitoring of language. Finally, the STG is fundamental in the perception of emotions in facial stimuli (Bigler et al., 2007; Radua et al., 2010) and has been reported to be important in the pathway consisting of the amygdala and prefrontal cortex, which are all involved in social cognitive processing (Adolphs, 2003; Bigler et al., 2007). Dysfunction of either the STG of its network of connections is pertinent to SCZ and has been closely linked to two key positive symptoms, auditory hallucinations and thought disorder (Allen et al., 2008; Pearlson, 1997; Shenton et al., 1992). Abnormalities of the temporal cortex are also well documented in patients with SCZ (Shenton et al., 2001; Wright et al., 2000). Reduced volumes of the STG have been reported (Barta et al., 1990; Hirayasu et al., 2000; Southard, 1910), particularly on the left side (O'donnell et al., 2004; Reite et al., 1997). Subregions of the STG such as the Heschl's gyrus and left planum temporale also show consistent abnormalities in SCZ (Honea et al., 2005; Kasai et al., 2003), and the severity of hallucinations has been reported to correlate with volume loss in the left Heschl's gyrus (Gaser et al., 2004). More consistent with our findings of increased C_{DEOXY} is that the relative metabolism in the STG of SCZ patients with hallucinations has been reported to be increased (Cleghorn et al., 1990; Horga et al., 2011; Nenadic et al., 2014), and blood flow to the left STG increased (Suzuki et al., 1993) in SCZ patients. Similar STG findings in BPD and SCZ in our study may reflect some genetic overlap between these disorders. STG findings however are less commonly observed in BPD (Anderson et al., 2013; Nenadic et al., 2015), although shared abnormalities between SCZ and BPD have been reported in some structural (Cui et al., 2011; Rimol et al., 2010), spectroscopic (Atagun et al., 2015) and electrophysiological (Wang et al., 2014) studies. STG abnormalities in unaffected siblings of schizophrenia patients have been found by some (Honea et al., 2008) but not other (Hu et al., 2013) authors. Our findings of increased STG C_{DEOXY} in SIB participants suggest that STG hyperactivity alone is not pathognomonic of SCZ, and may represent a genetic trait conferring some vulnerability to developing the illness.

Evidence for trait heritability may also be present in the thalamus, where increased C_{DEOXY} was noted in SCZ BPD, and SIB, and these effects appeared to be similarly present in either hemisphere. The main function of the thalamus is to relay motor and sensory signals to the cerebral cortex; but it also regulates sleep and alertness. Thalamic circuits feature prominently in theoretical models of SCZ, and are implicated in empirical SCZ studies. Structural thalamic abnormalities are sometimes found in SCZ and SIB (Harms et al., 2007; Mamah et al., 2010; Wang et al., 2008), and may represent a dysfunction in the processing of cortical sensory inputs (Pergola et al., 2015). While hypoconnectivity to prefrontal cortex in SCZ and those at clinical-risk for developing psychosis have been found (Anticevic et al., 2014; Klingner et al., 2014; Mamah et al., 2010; Woodward et al., 2012), increased thalamic connectivity with sensory–motor cortices, including those involved in visual and auditory processing (Anticevic et al., 2015; Damaraju et al., 2014; Hoffman et al., 2011; Klingner et al., 2014; Woodward et al., 2012), have also been reported. An increased thalamic C_{DEOXY} in SCZ, BPD an SIB in our study may thus indicate hyperactivity stemming from an aberrantly hyperconnected thalamocortical network. In the future, GEPCI relaxometric studies evaluating findings from individual thalamic nuclei may help clarify the specific thalamacortical pathways involved in psychiatric disorders.

C_{DEOXY} derived from GEPCI is unique since it quantifies brain activity by estimating the deoxyhemoglobin concentration. Furthermore, it provides an absolute measure of brain activity at rest, and not activity relative to another time period or specific task. Other methods for estimating brain activity, such as functional MRI approaches, primarily detect task-associated hemodynamic changes, which can be dependent on task design and administrator experience. Using selective radiotracers, positron emission tomography (PET) and single photon emission computer tomography (SPECT) imaging have also been used to estimate brain activity investigating blood flow or glucose metabolism. These methods while considered generally safe, also have some radiation risks, which can limit their use, and are generally time intensive. C_{DEOXY} as a measure of brain activity however has to be considered in the context of underlying cerebral blood flow (CBF), which can influence findings. As described in Eq. (6), C_{DEOXY} is proportional to $(1 - Y)$ which is directly related to the oxygen extraction fraction (OEF). OEF, in turn, is inversely proportional to the CBF (Yablonskiy et al., 2013a). Hence, the increase in measured regional C_{DEOXY} observed in our non-control groups may have potentially been the result of decreased CBF. Across studies, CBF findings have been variable with some to no abnormalities in different brain regions in SCZ

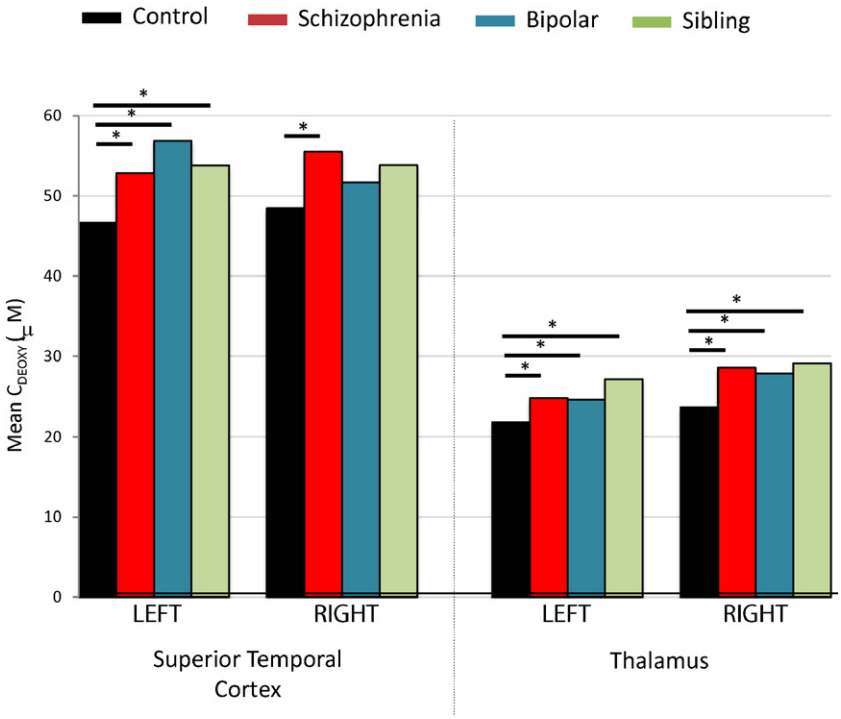

Fig. 3. Group C_{DEOXY} comparisons by hemisphere. Bars represent least square mean values of the median C_{DEOXY} value in each ROI, controlled for age. *p < 0.05 **p < 0.005.

(Pinkham et al., 2011; Talati et al., 2015; Zhu et al., 2015) or BPD (Blumberg et al., 2000; Bolwig, 1993; Silfverskiold and Risberg, 1989). Arterial spin labeling or SPECT has been used in previous SCZ studies, and have shown increased CBF in the left superior temporal gyrus (Homan et al., 2013; Suzuki et al., 1993), while decreased CBF have been reported on the right (Gonul et al., 2003). CBF abnormalities in the superior temporal gyrus of BPD patients have not been reported to our knowledge, although hyperperfusion of temporal regions have been described (Agarwal et al., 2008). Similarly in the thalamus, both increased (Kim et al., 2000; Lewis et al., 1992; Malaspina et al., 2004; Scheef et al., 2010) and decreased (Andreasen et al., 2008; Vita et al., 1995) CBF have been reported in SCZ. In future studies, blood flow measurement methods, such as arterial spin labeling, alongside GEPCI-based relaxometry could help clarify nature of C_{DEOXY} abnormality in patients.

Our study demonstrated that in SCZ, most brain regions had lower mean $R2^*_C$ than CON to some degree. However, we did not identify statistically significant group effects in gray matter $R2^*_C$ suggesting that no differences in cellular integrity exist across groups. This result however may have been due to insufficient group sizes, which can be addressed in larger studies. There are multiple known neuropathological findings that could cause $R2^*_C$ abnormalities. Low $R2^*_C$ (i.e. high $T2^*_C$) signaling can be associated with neurobiological alterations that are sometimes associated with psychiatric disorders, such as decreased myelination (Fields, 2008) or decreased cellular density secondary to neurodegeneration — including from apoptosis (Glantz et al., 2006; Jarskog et al., 2005) or small infarcts (Bruton et al., 1990; Jellinger, 1985; Riederer et al., 1995; Stevens, 1982). In addition, decreased size of neurons, neuronal processes and/or synaptic spines are often noted in neuropathologic studies (Elston and Rosa, 1998; Garey, 2010; Hayes and Lewis, 1996; Ho et al., 1992; Pierce and Lewin, 1994). Such findings have sometimes been associated with decreased cellular density in SCZ (Cotter et al., 2001; Di Rosa et al., 2009) or BPD (Cotter et al., 2005; Rajkowska et al., 2001). Unlike our findings in gray matter, we did not find any significant relaxometric abnormalities in total white matter in any non-control participants. This suggests an absence of major pathology in the white matter as a whole. Results however do not rule out the possibility of regional white matter abnormalities.

GEPCI relaxometric findings in SCZ cannot exclusively be ascribed to brain abnormalities intrinsic to the disorder itself. For example, several commonly used recreational substances including cannabis (Smith et al., 2014) and alcohol (Smith et al., 2011) can alter brain tissue architecture, and substance use disorder histories were more prevalent in the non-control groups, particularly in SCZ. However, our study was not optimally designed to uncover drug influences on relaxometric data, as the amount and length of substance use was not investigated. Medications can also differ in their effects on altering brain tissue structure (Mamah et al., 2012), although the presence of similar findings in unmedicated siblings of schizophrenia participants suggests that medication do not have a major role on C_{DEOXY}.

In summary, using GEPCI, our studies found increased C_{DEOXY} in most regions in the majority of ROIs of non-control participants, but most notably in the superior temporal cortex and thalamus. These findings could indicate that hyperactivity in these regions is part of the pathophysiology of schizophrenia and bipolar disorder. Conclusions from our studies are limited by the modest sample size, which can influence the power to detect significant group differences or clinical correlations. Larger studies involving GEPCI in related populations will therefore be necessary to validate findings. Including additional brain regions, such as the midbrain or cerebellum, will provide further information about pathologic processes that may be involved in psychiatric disorders. For example, midbrain dopaminergic neurons within the ventral tegmental area or substantia nigra may be abnormal in psychosis, and exhibit altered relaxometric properties suggesting hyperactivity (Watanabe et al., 2014). The clinical relevance of findings will also have to be studied using a more extensive assessment battery, including those evaluating mood symptoms and cognition. In addition, further studies are needed to help clarify the extent of heterogeneity in $R2^*$ abnormalities within psychiatric populations. Developments in GEPCI and related relaxometric methodologies will likely provide more

precise distinctions between underlying brain neuropathologies. Results of such studies could be valuable for selecting treatment and identifying those at risk for developing illness.

Role of the funding source

This research was supported by NIH grants P50 MH071616, R01 MH56584 and K08 MH085948.

Contributor

Daniel Mamah wrote the first draft of the manuscript. Barch oversaw statistical analyses. Wen, Luo and Ulrich conducted the GEPCI experiments. Yablonskiy developed the GEPCI methodology and oversaw its application to our study population.

Conflict of interest

Dr. Mamah has received grants from the NIMH, NARSAD, the McDonnell Center for Systems Neuroscience, the Taylor Family Institute and Eli Lilly. Dr. Barch has received grants from the NIMH, NIA, NARSAD, Allon, Novartis, and the McDonnell Center for Systems Neuroscience and has consulted for Pfizer.

Acknowledgments

This research was supported by NIH grants P50 MH071616, R01 MH56584 and K08 MH085948. Dr. Mamah has received grants from the NIMH, NARSAD, the McDonnell Center for Systems Neuroscience, the Taylor Family Institute and Eli Lilly. Dr. Barch has received grants from the NIMH, NIA, NARSAD, Allon, Novartis, and the McDonnell Center for Systems Neuroscience and has consulted for Pfizer.

References

Adolphs, R., 2003. Is the human amygdala specialized for processing social information? Ann. N. Y. Acad. Sci. 985, 326–340.

Agarwal, N., Bellani, M., Perlini, C., Rambaldelli, G., Atzori, M., Cerini, R., Vecchiato, F., Pozzi Mucelli, R., Andreone, N., Balestrieri, M., Tansella, M., Brambilla, P., 2008. Increased fronto-temporal perfusion in bipolar disorder. J. Affect. Disord. 110 (1–2), 106–114.

Allen, P., Laroi, F., McGuire, P.K., Aleman, A., 2008. The hallucinating brain: a review of structural and functional neuroimaging studies of hallucinations. Neurosci. Biobehav. Rev. 32 (1), 175–191.

Anderson, D., Ardekani, B.A., Burdick, K.E., Robinson, D.G., John, M., Malhotra, A.K., Szeszko, P.R., 2013. Overlapping and distinct gray and white matter abnormalities in schizophrenia and bipolar I disorder. Bipolar Disord. 15 (6), 680–693.

Andreasen, N.C., Arndt, S., Alliger, R., Miller, D., Flaum, M., 1995. Symptoms of schizophrenia: methods, meanings, and mechanisms. Arch. Gen. Psychiatry 52, 341–351.

Andreasen, N.C., Calarge, C.A., O'Leary, D.S., 2008. Theory of mind and schizophrenia: a positron emission tomography study of medication-free patients. Schizophr. Bull. 34 (4), 708–719.

Anticevic, A., Cole, M.W., Repovs, G., Murray, J.D., Brumbaugh, M.S., Winkler, A.M., Savic, A., Krystal, J.H., Pearlson, G.D., Glahn, D.C., 2014. Characterizing thalamo-cortical disturbances in schizophrenia and bipolar illness. Cereb. Cortex 24 (12), 3116–3130.

Anticevic, A., Haut, K., Murray, J.D., Repovs, G., Yang, G.J., Diehl, C., McEwen, S.C., Bearden, C.E., Addington, J., Goodyear, B., Cadenhead, K.S., Mirzakhanian, H., Cornblatt, B.A., Olvet, D., Mathalon, D.H., McGlashan, T.H., Perkins, D.O., Belger, A., Seidman, L.J., Tsuang, M.T., van Erp, T.G., Walker, E.F., Hamann, S., Woods, S.W., Qiu, M., Cannon, T.D., 2015. Association of thalamic dysconnectivity and conversion to psychosis in youth and young adults at elevated clinical risk. JAMA Psychiatry 72 (9), 882–891.

Arnold, S.E., 2000. Cellular and molecular neuropathology of the parahippocampal region in schizophrenia. Ann. N. Y. Acad. Sci. 911, 275–292.

Arnold, S.E., Trojanowski, J.Q., 1996. Recent advances in defining the neuropathology of schizophrenia. Acta Neuropathol. 92 (3), 217–231.

Arnold, S.E., Franz, B.R., Trojanowski, J.Q., Moberg, P.J., Gur, R.E., 1996. Glial fibrillary acidic protein-immunoreactive astrocytosis in elderly patients with schizophrenia and dementia. Acta Neuropathol. 91 (3), 269–277.

Atagun, M.I., Sikoglu, E.M., Can, S.S., Karakas-Ugurlu, G., Ulusoy-Kaymak, S., Caykoylu, A., Algin, O., Phillips, M.L., Moore, C.M., Ongur, D., 2015. Investigation of Heschl's gyrus and planum temporale in patients with schizophrenia and bipolar disorder: a proton magnetic resonance spectroscopy study. Schizophr. Res. 161 (2–3), 202–209.

Barta, P.E., Pearlson, G.D., Powers, R.E., Richards, S.S., Tune, L.E., 1990. Auditory hallucinations and smaller superior temporal gyral volume in schizophrenia. Am. J. Psychiatry 147 (11), 1457–1462.

Bigler, E.D., Mortensen, S., Neeley, E.S., Ozonoff, S., Krasny, L., Johnson, M., Lu, J., Provencal, S.L., McMahon, W., Lainhart, J.E., 2007. Superior temporal gyrus, language function, and autism. Dev. Neuropsychol. 31 (2), 217–238.

Blumberg, H.P., Stern, E., Martinez, D., Ricketts, S., de Asis, J., White, T., Epstein, J., McBride, P.A., Eidelberg, D., Kocsis, J.H., Silbersweig, D.A., 2000. Increased anterior cingulate and caudate activity in bipolar mania. Biol. Psychiatry 48 (11), 1045–1052.

Bolwig, T.G., 1993. Regional cerebral blood flow in affective disorder. Acta Psychiatr. Scand. Suppl. 371, 48–53.

Bruton, C.J., Crow, T.J., Frith, C.D., Johnstone, E.C., Owens, D.G., Roberts, G.W., 1990. Schizophrenia and the brain: a prospective clinico-neuropathological study. Psychol. Med. 20 (2), 285–304.

Casanova, M.F., Stevens, J.R., Kleinman, J.E., 1990. Astrocytosis in the molecular layer of the dentate gyrus: a study in Alzheimer's disease and schizophrenia. Psychiatry Res. 35 (2), 149–166.

Cleghorn, J.M., Garnett, E.S., Nahmias, C., Brown, G.M., Kaplan, R.D., Szechtman, H., Szechtman, B., Franco, S., Dermer, S.W., Cook, P., 1990. Regional brain metabolism during auditory hallucinations in chronic schizophrenia. Br. J. Psychiatry 157, 562–570.

Cotter, D., Hudson, L., Landau, S., 2005. Evidence for orbitofrontal pathology in bipolar disorder and major depression, but not in schizophrenia. Bipolar Disord. 7 (4), 358–369.

Cotter, D., Mackay, D., Landau, S., Kerwin, R., Everall, I., 2001. Reduced glial cell density and neuronal size in the anterior cingulate cortex in major depressive disorder. Arch. Gen. Psychiatry 58 (6), 545–553.

Cui, L., Li, M., Deng, W., Guo, W., Ma, X., Huang, C., Jiang, L., Wang, Y., Collier, D.A., Gong, Q., Li, T., 2011. Overlapping clusters of gray matter deficits in paranoid schizophrenia and psychotic bipolar mania with family history. Neurosci. Lett. 489 (2), 94–98.

Cullen, T.J., Walker, M.A., Eastwood, S.L., Esiri, M.M., Harrison, P.J., Crow, T.J., 2006. Anomalies of asymmetry of pyramidal cell density and structure in dorsolateral prefrontal cortex in schizophrenia. Br. J. Psychiatry 188, 26–31.

Damaraju, E., Allen, E.A., Belger, A., Ford, J.M., McEwen, S., Mathalon, D.H., Mueller, B.A., Pearlson, G.D., Potkin, S.G., Preda, A., Turner, J.A., Vaidya, J.G., van Erp, T.G., Calhoun, V.D., 2014. Dynamic functional connectivity analysis reveals transient states of dysconnectivity in schizophrenia. NeuroImage: Clinical 5, 298–308.

Derdeyn, C.P., Videen, T.O., Yundt, K.D., Fritsch, S.M., Carpenter, D.A., Grubb, R.L., Powers, W.J., 2002. Variability of cerebral blood volume and oxygen extraction: stages of cerebral haemodynamic impairment revisited. Brain 125 (Pt 3), 595–607.

Di Rosa, E., Crow, T.J., Walker, M.A., Black, G., Chance, S.A., 2009. Reduced neuron density, enlarged minicolumn spacing and altered ageing effects in fusiform cortex in schizophrenia. Psychiatry Res. 166 (2–3), 102–115.

Elston, G.N., Rosa, M.G., 1998. Morphological variation of layer III pyramidal neurones in the occipitotemporal pathway of the macaque monkey visual cortex. Cereb. Cortex 8 (3), 278–294.

Fields, R.D., 2008. White matter in learning, cognition and psychiatric disorders. Trends Neurosci. 31 (7), 361–370.

Garey, L., 2010. When cortical development goes wrong: schizophrenia as a neurodevelopmental disease of microcircuits. J. Anat. 217 (4), 324–333.

Gaser, C., Nenadic, I., Volz, H.P., Buchel, C., Sauer, H., 2004. Neuroanatomy of 'hearing voices': a frontotemporal brain structural abnormality associated with auditory hallucinations in schizophrenia. Cereb. Cortex 14 (1), 91–96.

Glantz, L.A., Gilmore, J.H., Lieberman, J.A., Jarskog, L.F., 2006. Apoptotic mechanisms and the synaptic pathology of schizophrenia. Schizophr. Res. 81 (1), 47–63.

Gonul, A.S., Kula, M., Esel, E., Tutus, A., Sofuoglu, S., 2003. A Tc-99m HMPAO SPECT study of regional cerebral blood flow in drug-free schizophrenic patients with deficit and non-deficit syndrome. Psychiatry Res. 123 (3), 199–205.

Harms, M.P., Wang, L., Mamah, D., Barch, D.M., Thompson, P.A., Csernansky, J.G., 2007. Thalamic shape abnormalities in individuals with schizophrenia and their nonpsychotic siblings. J. Neurosci. 27 (50), 13,835–13,842.

Hayes, T.L., Lewis, D.A., 1996. Magnopyramidal neurons in the anterior motor speech region. Dendritic features and interhemispheric comparisons. Arch. Neurol. 53 (12), 1277–1283.

He, X., Yablonskiy, D.A., 2007. Quantitative BOLD: mapping of human cerebral deoxygenated blood volume and oxygen extraction fraction: default state. Magn. Reson. Med. 57 (1), 115–126.

Hirayasu, Y., McCarley, R.W., Salisbury, D.F., Tanaka, S., Kwon, J.S., Frumin, M., Snyderman, D., Yurgelun-Todd, D., Kikinis, R., Jolesz, F.A., Shenton, M.E., 2000. Planum temporale and Heschl gyrus volume reduction in schizophrenia — a magnetic resonance imaging study of first-episode patients. Arch. Gen. Psychiatry 57 (7), 692–699.

Ho, K.C., Gwozdz, J.T., Hause, L.L., Antuono, P.G., 1992. Correlation of neuronal cell body size in motor cortex and hippocampus with body height, body weight, and axonal length. Int. J. Neurosci. 65 (1–4), 147–153.

Hoffman, R.E., Fernandez, T., Pittman, B., Hampson, M., 2011. Elevated functional connectivity along a corticostriatal loop and the mechanism of auditory/verbal hallucinations in patients with schizophrenia. Biol. Psychiatry 69 (5), 407–414.

Homan, P., Kindler, J., Hauf, M., Walther, S., Hubl, D., Dierks, T., 2013. Repeated measurements of cerebral blood flow in the left superior temporal gyrus reveal tonic hyperactivity in patients with auditory verbal hallucinations: a possible trait marker. Front. Hum. Neurosci. 7, 304.

Honea, R., Crow, T.J., Passingham, D., Mackay, C.E., 2005. Regional deficits in brain volume in schizophrenia: a meta-analysis of voxel-based morphometry studies. Am. J. Psychiatry 162 (12), 2233–2245.

Honea, R.A., Meyer-Lindenberg, A., Hobbs, K.B., Pezawas, L., Mattay, V.S., Egan, M.F., Verchinski, B., Passingham, R.E., Weinberger, D.R., Callicott, J.H., 2008. Is gray matter volume an intermediate phenotype for schizophrenia? A voxel-based morphometry study of patients with schizophrenia and their healthy siblings. Biol. Psychiatry 63 (5), 465–474.

Horga, G., Parellada, E., Lomena, F., Fernandez-Egea, E., Mane, A., Font, M., Falcon, C., Konova, A.B., Pavia, J., Ros, D., Bernardo, M., 2011. Differential brain glucose metabolic patterns in antipsychotic-naive first-episode schizophrenia with and without auditory verbal hallucinations. J. Psychiatry Neurosci. 36 (5), 312–321.

Hu, M., Li, J., Eyler, L., Guo, X., Wei, Q., Tang, J., Liu, F., He, Z., Li, L., Jin, H., Liu, Z., Wang, J., Liu, F., Chen, H., Zhao, J., 2013. Decreased left middle temporal gyrus volume in antipsychotic drug-naive, first-episode schizophrenia patients and their healthy unaffected siblings. Schizophr. Res. 144 (1–3), 37–42.

Iadecola, C., 2004. Neurovascular regulation in the normal brain and in Alzheimer's disease. Nat. Rev. Neurosci. 5 (5), 347–360.

Jarskog, L.F., Glantz, L.A., Gilmore, J.H., Lieberman, J.A., 2005. Apoptotic mechanisms in the pathophysiology of schizophrenia. Prog. Neuro-Psychopharmacol. Biol. Psychiatry 29 (5), 846–858.

Jellinger, K., 1985. Neuromorphological background of pathochemical studies in major psychoses. In: Beckmann, H., Riederer, P. (Eds.), Pathochemical markers in mauor psychoses. Springer, Berlin.

Jenkinson, M., Bannister, P., Brady, M., Smith, S., 2002. Improved optimization for the robust and accurate linear registration and motion correction of brain images. NeuroImage 17 (2), 825–841.
Jenkinson, M., Beckmann, C.F., Behrens, T.E.J., Woolrich, M.W., Smith, S.M., 2012. FSL. NeuroImage 62 (2), 782–790.
Karnath, H.O., 2001. New insights into the functions of the superior temporal cortex. Nat. Rev. Neurosci. 2 (8), 568–576.
Kasai, K., Shenton, M.E., Salisbury, D.F., Hirayasu, Y., Onitsuka, T., Spencer, M.H., Yurgelun-Todd, D.A., Kikinis, R., Jolesz, F.A., McCarley, R.W., 2003. Progressive decrease of left Heschl gyrus and planum temporale gray matter volume in first-episode schizophrenia — a longitudinal magnetic resonance imaging study. Arch. Gen. Psychiatry 60 (8), 766–775.
Kim, J.J., Mohamed, S., Andreasen, N.C., O'Leary, D.S., Watkins, G.L., Boles Ponto, L.L., Hichwa, R.D., 2000. Regional neural dysfunctions in chronic schizophrenia studied with positron emission tomography. Am. J. Psychiatry 157 (4), 542–548.
Klingner, C.M., Langbein, K., Dietzek, M., Smesny, S., Witte, O.W., Sauer, H., Nenadic, I., 2014. Thalamocortical connectivity during resting state in schizophrenia. Eur. Arch. Psychiatry Clin. Neurosci. 264 (2), 111–119.
Lewis, S.W., Ford, R.A., Syed, G.M., Reveley, A.M., Toone, B.K., 1992. A controlled study of 99mTc-HMPAO single-photon emission imaging in chronic schizophrenia. Psychol. Med. 22 (1), 27–35.
Luo, J., Jagadeesan, B.D., Cross, A.H., Yablonskiy, D.A., 2012. Gradient Echo Plural Contrast Imaging — signal model and derived contrasts: T2*, T1, Phase, SWI, T1f, FST2*and T2*-SWI. NeuroImage 60 (2), 1073–1082.
Luo, J., Yablonskiy, D.A., Hildebolt, C.F., Lancia, S., Cross, A.H., 2014. Gradient echo magnetic resonance imaging correlates with clinical measures and allows visualization of veins within multiple sclerosis lesions. Mult. Scler. 20 (3), 349–355.
Malaspina, D., Harkavy-Friedman, J., Corcoran, C., Mujica-Parodi, L., Printz, D., Gorman, J.M., Van Heertum, R., 2004. Resting neural activity distinguishes subgroups of schizophrenia patients. Biol. Psychiatry 56 (12), 931–937.
Mamah, D., Conturo, T.E., Harms, M.P., Akbudak, E., Wang, L., McMichael, A.R., Gado, M.H., Barch, D.M., Csernansky, J.G., 2010. Anterior thalamic radiation integrity in schizophrenia: a diffusion-tensor imaging study. Psychiatry Res. 183 (2), 144–150.
Mamah, D., Harms, M.P., Barch, D., Styner, M., Lieberman, J.A., Wang, L., 2012. Hippocampal shape and volume changes with antipsychotics in early stage psychotic illness. Front. Psychol. 3, 96.
Nenadic, I., Dietzek, M., Langbein, K., Rzanny, R., Gussew, A., Reichenbach, J.R., Sauer, H., Smesny, S., 2014. Superior temporal metabolic changes related to auditory hallucinations: a (31)P-MR spectroscopy study in antipsychotic-free schizophrenia patients. Brain Struct. Funct. 219 (5), 1869–1872.
Nenadic, I., Maitra, R., Langbein, K., Dietzek, M., Lorenz, C., Smesny, S., Reichenbach, J.R., Sauer, H., Gaser, C., 2015. Brain structure in schizophrenia vs. psychotic bipolar I disorder: a VBM study. Schizophr. Res. 165 (2–3), 212–219.
O'donnell, B.F., Vohs, J.L., Hetrick, W.P., Carroll, C.A., Shekhar, A., 2004. Auditory event-related potential abnormalities in bipolar disorder and schizophrenia. Int. J. Psychophysiol. 53 (1), 45–55.
Ogawa, S., 2012. Finding the BOLD effect in brain images. NeuroImage 62 (2), 608–609.
Pearlson, G.D., 1997. Superior temporal gyrus and planum temporale in schizophrenia: a selective review. Prog. Neuro-Psychopharmacol. Biol. Psychiatry 21 (8), 1203–1229.
Pergola, G., Selvaggi, P., Trizio, S., Bertolino, A., Blasi, G., 2015. The role of the thalamus in schizophrenia from a neuroimaging perspective. Neurosci. Biobehav. Rev. 54, 57–75.
Pierce, J.P., Lewin, G.R., 1994. An ultrastructural size principle. Neuroscience 58 (3), 441–446.
Pinkham, A., Loughead, J., Ruparel, K., Wu, W.C., Overton, E., Gur, R., Gur, R., 2011. Resting quantitative cerebral blood flow in schizophrenia measured by pulsed arterial spin labeling perfusion MRI. Psychiatry Res. 194 (1), 64–72.
Quirk, J.D., Sukstanskii, A.L., Bretthorst, G.L., Yablonskiy, D.A., 2009. Optimal decay rate constant estimates from phased array data utilizing joint Bayesian analysis. J. Magn. Reson. 198 (1), 49–56.
Radua, J., Phillips, M.L., Russell, T., Lawrence, N., Marshall, N., Kalidindi, S., El-Hage, W., McDonald, C., Giampietro, V., Brammer, M.J., David, A.S., Surguladze, S.A., 2010. Neural response to specific components of fearful faces in healthy and schizophrenic adults. NeuroImage 49 (1), 939–946.
Raichle, M.E., Mintun, M.A., 2006. Brain work and brain imaging. Annu. Rev. Neurosci. 29, 449–476.
Rajkowska, G., Halaris, A., Selemon, L.D., 2001. Reductions in neuronal and glial density characterize the dorsolateral prefrontal cortex in bipolar disorder. Biol. Psychiatry 49 (9), 741–752.
Reite, M., Sheeder, J., Teale, P., Adams, M., Richardson, D., Simon, J., Jones, R.H., Rojas, D.C., 1997. Magnetic source imaging evidence of sex differences in cerebral lateralization in schizophrenia. Arch. Gen. Psychiatry 54 (5), 433–440.
Riederer, P., Gsell, W., Calza, L., Franzek, E., Jungkunz, G., Jellinger, K., Reynolds, G.P., Crow, T., Cruz-Sanchez, F.F., Beckmann, H., 1995. Consensus on minimal criteria of clinical and neuropathological diagnosis of schizophrenia and affective disorders for post mortem research. Report from the European Dementia and Schizophrenia Network (BIOMED I). J. Neural Transm. Gen. Sect. 102 (3), 255–264.
Rimol, L.M., Hartberg, C.B., Nesvag, R., Fennema-Notestine, C., Hagler Jr., D.J., Pung, C.J., Jennings, R.G., Haukvik, U.K., Lange, E., Nakstad, P.H., Melle, I., Andreassen, O.A., Dale, A.M., Agartz, I., 2010. Cortical thickness and subcortical volumes in schizophrenia and bipolar disorder. Biol. Psychiatry 68 (1), 41–50.
Roberts, G.W., Colter, N., Lofthouse, R., Bogerts, B., Zech, M., Crow, T.J., 1986. Gliosis in schizophrenia: a survey. Biol. Psychiatry 21 (11), 1043–1050.
Ropele, S., Wattjes, M.P., Langkammer, C., Kilsdonk, I.D., de Graaf, W.L., Frederiksen, J.L., Fuglo, D., Yiannakas, M., Wheeler-Kingshott, C.A., Enzinger, C., Rocca, M.A., Sprenger, T., Amman, M., Kappos, L., Filippi, M., Rovira, A., Ciccarelli, O., Barkhof, F., Fazekas, F., 2013. Multicenter R2* mapping in the healthy brain. Magn. Reson. Med.
Sati, P., Cross, A.H., Luo, J., Hildebolt, C.F., Yablonskiy, D.A., 2010. In vivo quantitative evaluation of brain tissue damage in multiple sclerosis using Gradient Echo Plural Contrast Imaging technique. NeuroImage 51 (3), 1089–1097.
Scheef, L., Manka, C., Daamen, M., Kuhn, K.U., Maier, W., Schild, H.H., Jessen, F., 2010. Resting-state perfusion in nonmedicated schizophrenic patients: a continuous arterial spin-labeling 3.0-T MR study. Radiology 256 (1), 253–260.
Schlaug, G., Armstrong, E., Schleicher, A., Zilles, K., 1993. Layer V pyramidal cells in the adult human cingulate cortex. A quantitative Golgi-study. Anat. Embryol. 187 (6), 515–522.
Selemon, L.D., 2001. Regionally diverse cortical pathology in schizophrenia: clues to the etiology of the disease. Schizophr. Bull. 27 (3), 349–377.
Shenton, M.E., Dickey, C.C., Frumin, M., McCarley, R.W., 2001. A review of MRI findings in schizophrenia. Schizophr. Res. 49 (1–2), 1–52.
Shenton, M.E., Kikinis, R., Jolesz, F.A., Pollak, S.D., LeMay, M., Wible, C.G., Hokama, H., Martin, J., Metcalf, D., Coleman, M., et al., 1992. Abnormalities of the left temporal lobe and thought disorder in schizophrenia. A quantitative magnetic resonance imaging study. N. Engl. J. Med. 327 (9), 604–612.
Silfverskiold, P., Risberg, J., 1989. Regional cerebral blood flow in depression and mania. Arch. Gen. Psychiatry 46 (3), 253–259.
Smith, M.J., Cobia, D.J., Wang, L., Alpert, K.I., Cronenwett, W.J., Goldman, M.B., Mamah, D., Barch, D.M., Breiter, H.C., Csernansky, J.G., 2014. Cannabis-related working memory deficits and associated subcortical morphological differences in healthy individuals and schizophrenia subjects. Schizophr. Bull. 40 (2), 287–299.
Smith, M.J., Wang, L., Cronenwett, W., Goldman, M.B., Mamah, D., Barch, D.M., Csernansky, J.G., 2011. Alcohol use disorders contribute to hippocampal and subcortical shape differences in schizophrenia. Schizophr. Res. 131 (1–3), 174–183.
Southard, E.E., 1910. A study of the dementia praecox group in the light of certain cases showing anomalies or scleroses in particular brain-regions. Am. J. Insanity 67 (1), 119–176.
Spees, W.M., Yablonskiy, D.A., Oswood, M.C., Ackerman, J.J., 2001. Water proton MR properties of human blood at 1.5 Tesla: magnetic susceptibility, T(1), T(2), T*(2), and non-Lorentzian signal behavior. Magn. Reson. Med. 45 (4), 533–542.
Stevens, J.R., 1982. Neuropathology of schizophrenia. Arch. Gen. Psychiatry 39 (10), 1131–1139.
Stevens, C.D., Altshuler, L.L., Bogerts, B., Falkai, P., 1988. Quantitative study of gliosis in schizophrenia and Huntington's chorea. Biol. Psychiatry 24 (6), 697–700.
Sun, J., Maller, J.J., Guo, L., Fitzgerald, P.B., 2009. Superior temporal gyrus volume change in schizophrenia: a review on region of interest volumetric studies. Brain Res. Rev. 61 (1), 14–32.
Suzuki, M., Yuasa, S., Minabe, Y., Murata, M., Kurachi, M., 1993. Left superior temporal blood flow increases in schizophrenic and schizophreniform patients with auditory hallucination: a longitudinal case study using 123I-IMP SPECT. Eur. Arch. Psychiatry Clin. Neurosci. 242 (5), 257–261.
Talati, P., Rane, S., Skinner, J., Gore, J., Heckers, S., 2015. Increased hippocampal blood volume and normal blood flow in schizophrenia. Psychiatry Res. 232 (3), 219–225.
Ulrich, X., Yablonskiy, D.A., 2015. Separation of cellular and BOLD contributions to T2* signal relaxation. Magn. Reson. Med.
Vita, A., Bressi, S., Perani, D., Invernizzi, G., Giobbio, G.M., Dieci, M., Garbarini, M., Del Sole, A., Fazio, F., 1995. High-resolution SPECT study of regional cerebral blood flow in drug-free and drug-naive schizophrenic patients. Am. J. Psychiatry 152 (6), 876–882.
Wang, Y., Jia, Y., Feng, Y., Zhong, S., Xie, Y., Wang, W., Guan, Y., Zhu, D., Huang, L., 2014. Overlapping auditory M100 and M200 abnormalities in schizophrenia and bipolar disorder: a MEG study. Schizophr. Res. 160 (1–3), 201–207.
Wang, L., Mamah, D., Harms, M.P., Karnik, M., Price, J.L., Gado, M.H., Thompson, P.A., Barch, D.M., Miller, M.I., Csernansky, J.G., 2008. Progressive deformation of deep brain nuclei and hippocampal-amygdala formation in schizophrenia. Biol. Psychiatry 64 (12), 1060–1068.
Watanabe, Y., Tanaka, H., Tsukabe, A., Kunitomi, Y., Nishizawa, M., Hashimoto, R., Yamamori, H., Fujimoto, M., Fukunaga, M., Tomiyama, N., 2014. Neuromelanin magnetic resonance imaging reveals increased dopaminergic neuron activity in the substantia nigra of patients with schizophrenia. PLoS One 9 (8), e104619.
Weiskopf, N., Suckling, J., Williams, G., Correia, M.M., Inkster, B., Tait, R., Ooi, C., Bullmore, E.T., Lutti, A., 2013. Quantitative multi-parameter mapping of R1, PD(*), MT, and R2(*) at 3 T: a multi-center validation. Front. Neurosci. 7, 95.
Wen, J., Cross, A.H., Yablonskiy, D.A., 2014. On the role of physiological fluctuations in quantitative gradient echo MRI: implications for GEPCI, QSM, and SWI. Magn. Reson. Med.
Wen, J., Yablonskiy, D.A., Luo, J., Lancia, S., Hildebolt, C., Cross, A.H., 2015. Detection and quantification of regional cortical gray matter damage in multiple sclerosis utilizing gradient echo MRI. NeuroImage: Clinical 9, 164–175.
Whiteford, H.A., Degenhardt, L., Rehm, J., Baxter, A.J., Ferrari, A.J., Erskine, H.E., Charlson, F.J., Norman, R.E., Flaxman, A.D., Johns, N., Burstein, R., Murray, C.J., Vos, T., 2013. Global burden of disease attributable to mental and substance use disorders: findings from the Global Burden of Disease Study 2010. Lancet 382 (9904), 1575–1586.
Woodward, N.D., Karbasforoushan, H., Heckers, S., 2012. Thalamocortical dysconnectivity in schizophrenia. Am. J. Psychiatry 169 (10), 1092–1099.
Wright, I.C., Rabe-Hesketh, S., Woodruff, P.W., David, A.S., Murray, R.M., Bullmore, E.T., 2000. Meta-analysis of regional brain volumes in schizophrenia. Am. J. Psychiatry 157 (1), 16–25.
Yablonskiy, D.A., 1998. Quantitation of intrinsic magnetic susceptibility-related effects in a tissue matrix. Phantom study. Magn. Reson. Med. 39 (3), 417–428.

Yablonskiy, D.A., 2000. Gradient Echo Plural Contrast Imaging (GEPCI) — new fast magnetic resonance imaging technique for simultaneous acquisition of T2, T1 (or spin density) and T2*-weighted images. Radiology 217, 204.
Yablonskiy, D.A., Haacke, E.M., 1994. Theory of NMR signal behavior in magnetically inhomogeneous tissues: the static dephasing regime. Magn. Reson. Med. 32 (6), 749–763.
Yablonskiy, D.A., Sukstanskii, A.L., He, X., 2013a. Blood oxygenation level-dependent (BOLD)-based techniques for the quantification of brain hemodynamic and metabolic properties — theoretical models and experimental approaches. NMR Biomed. 26 (8), 963–986.
Yablonskiy, D.A., Sukstanskii, A.L., Luo, J., Wang, X., 2013b. Voxel spread function method for correction of magnetic field inhomogeneity effects in quantitative gradient-echo-based MRI. Magn. Reson. Med. 70 (5), 1283–1292.
Yablonskiy, D.A., Luo, J., Sukstanskii, A.L., Iyer, A., Cross, A.H., 2012. Biophysical mechanisms of MRI signal frequency contrast in multiple sclerosis. Proc. Natl. Acad. Sci. U. S. A. 109 (35), 14,212–14,217.
Zhu, J., Zhuo, C., Qin, W., Xu, Y., Xu, L., Liu, X., Yu, C., 2015. Altered resting-state cerebral blood flow and its connectivity in schizophrenia. J. Psychiatry Res. 63, 28–35.